

## Discretization Requirements: How many Elements per Wavelength are Necessary?

Steffen Marburg

Institut für Festkörpermechanik, Technische Universität Dresden,  
01062 Dresden, Germany  
marburg@ifkm.mw.tu-dresden.de

**Summary.** The commonly applied rule of thumb to use a fixed number of elements per wavelength in linear time-harmonic acoustics is discussed together with the question of using either continuous or discontinuous elements for collocation. Continuous interpolation of the sound pressure has been favored in most applications of boundary element methods for acoustics. Only a few papers are known where discontinuous elements are applied because they guarantee  $C^1$  continuity of the geometry at element edges. In these cases, it was assumed that the same number of elements as for continuous elements is required for the same numeric error. Of course this implies a larger degree of freedom. An effect of superconvergence is known for boundary element collocation on discontinuous elements. This effect is observed if the collocation points are located at the zeros of orthogonal functions, e.g. at the zeros of the Legendre polynomials. We start with a review of continuous and discontinuous boundary elements using constant, linear and quadratic interpolation on triangular and quadrilateral elements. Major part of this contribution consists of the investigation of the computational example of a long duct. For that, the numeric solution is compared with the analytic solution of the corresponding one-dimensional problem. Error dependence in terms of frequency, element size and location of nodes on discontinuous elements is reported. It will be shown that the zeros of the Legendre polynomials account for an optimal position of nodes for this problem of interior acoustics. Similar results are observed for triangular elements. It can be seen that the error in the Euclidean norm changes by one or two orders of magnitude if the location of nodes is shifted over the element. The irregular mesh of a sedan cabin compartment accounts for the second example. The optimal choice of node position is confirmed for this example. It is one of the key results of this paper, that discontinuous boundary elements perform more efficiently than continuous ones, in particular for linear elements. This, however, implies that nodes are located at the zeros of orthogonal functions on the element. Furthermore, there is no indication of a similarity to the pollution effect which is known from finite element methods.

### 11.1 Introduction

It is widely accepted that the element size in element-based acoustic computations should be related to the wavelength. Often, the element size is measured in a certain (fixed) number of elements per wavelength. In many cases, this number of elements per wavelength is given for constant or linear/bilinear elements. It varies between six

and ten. Obviously, this number is closely related to a certain desired accuracy. Often the error is of an acceptable magnitude which depends on the user and which meets certain technical requirements.

The idea of using a fixed number of elements per wavelength is most likely a consequence of Shannon's sampling theorem [14]. This theorem is of fundamental importance in vibration and acoustics for experimental measurements and frequency detection. It states that at least two points per wavelength (or period of oscillating function) are necessary to detect the corresponding frequency. However, a simple detection cannot be sufficient to approximate the function. Schmiechen [29] investigates discretization of axisymmetric structures for modal analysis. He states that two points per wavelength are strictly sufficient, but would still not lead to accurate mode shapes. Another factor of 3 to 5 is advised. This is equivalent to the number of six to ten nodes per wavelength. We mention that the number of nodes was given for bilinear shell elements. A similar result can be extracted from the author's paper [19]. There, the eigenvalues of a one-dimensional problem are shown for linear and quadratic finite elements. The eigenvalue distribution can be easily related to the Shannon frequency. For linear and quadratic elements, the largest eigenfrequency is slightly larger than the frequency which corresponds to two points per wavelength. For quadratic elements, a gap of eigenfrequencies occurs beyond frequencies of two (quadratic) elements per wavelength. This, however, is equivalent to four points per wave. Although done for finite elements this investigation will most likely hold for boundary element methods as well.

The common rule of using six linear boundary elements per wavelength (or, more general, six points per wavelength) are investigated in the author's papers [18, 22]. Therein, performance of constant elements, of linear and quadratic boundary elements are compared. The results of these papers are summarized in this article.

In boundary element methods, it is quite common to use Lagrangian elements [7, 8, 15, 36]. In contradiction to finite element methods, the basis functions of the boundary element method underly lower continuity requirements, i.e. there is no particular reason of demanding continuity at element edges for boundary element collocation methods. Consequently, the elements can be either continuous or discontinuous. This means that the physical quantity, i.e. the sound pressure may be either continuous or discontinuous at element edges but the geometry remains continuous. There are numerous examples of the use of discontinuous boundary elements in literature, cf. [1, 2, 9–12, 16, 17, 20, 23, 25–28, 30, 32, 33, 35, 37–40]. In many cases, discontinuous boundary elements have been used for collocation only because the normal derivative integral equation which requires  $C^1$ -continuity in the collocation point. This is relevant for methods such as the one by Burton and Miller [4, 24, 27]. Wu and Seybert [38, 39] proposed a discontinuous variant of using continuous interpolation while the collocation points were located inside the elements. This resulted in an overdetermined system of equations for the hypersingular formulation. In their review paper on DtN-methods for acoustic scattering and radiation, Harari et al. [11] mentioned that the hypersingular formulation of the boundary element method for wave scattering and radiation would be inefficient since necessity of discontinuous elements would require much more memory and computational time than conven-

tional boundary element methods that encounter the problem of the so-called irregular frequencies. This remark presupposes that the numeric error of discontinuous elements is about the same as for continuous elements while the degree of freedom is much higher for discontinuous interpolation. Similarly, same accuracy was presumed for continuous and discontinuous boundary elements in an older paper of Harari and Hughes [12] where efficiency of finite and boundary element methods was compared.

There are a number of papers in which discontinuous elements are compared with continuous elements. Often, continuous elements are considered advantageous, especially because they physical continuity condition at element edges is fulfilled [17,40]. For that reason, discontinuous elements were considered as an alternative to continuous elements if either higher continuity in the collocation point is required (see above) or if boundary conditions are discontinuous [17, 26]. In the paper [40] performance of discontinuous elements is evaluated based on the element-to-element jump of the physical quantity. Many authors (of engineering) conclude that they recommend the use of mixed continuous/discontinuous elements, i.e. discontinuous elements only where they are really required, but an overall mesh of discontinuous elements would supply too many degrees of freedom. The idea of using these mixed meshes is nicely worked out and presented in detail by do Rego Silva et al. [27, 28]. The element definitions given are will be reviewed here.

Herein, we will compare meshes of continuous and discontinuous elements based on the overall error arising due to a certain element size. It will be shown that discontinuous elements may give much smaller errors even for the same degree of freedom as a mesh of continuous elements. This is due to a superconvergence effect which has been well-known in mathematical literature.

Atkinson [2] reviewed this effect of superconvergence for error dependence upon element size for discontinuous boundary elements for the case that collocation points are located at the zeros of orthogonal functions for the standard interval. This effect had been discovered earlier by Chandler [5] and Chatelin and Lebbar [6]. Although this superconvergence effect was studied well, discontinuous boundary elements with nodes at zeros of orthogonal functions, in particular of Legendre polynomials as the simplest case, have hardly been used for practical applications. The authors have found very few papers that described this technique for the Helmholtz equation. A similar idea was proposed by Branski [3] who applied Čebyčev polynomials for acoustic source modeling. Tadeu and Antonio [32] found for the axisymmetric case that linear discontinuous elements are substantially influenced by position of collocation points whereas quadratic elements showed marginal dependence upon their locations. Extended investigations on continuous and discontinuous elements were presented in the aforementioned papers [18, 22]. The dependence on location of the collocation points on the element shows a clear optimum.

This paper is organized as follows: We start with the review of continuous and discontinuous Lagrangian boundary elements. These elements are compared with respect to two examples. The first considers traveling waves in a long duct. The numerical solution of the 3d-problem is compared with the simple analytic solution of the 1d-problem. A sedan cabin compartment is investigated as the second example.

## 11.2 Continuous and Discontinuous Boundary Elements

### 11.2.1 Quadrilateral Elements

Quadrilateral boundary elements are usually transformed from a standard interval  $-1 \leq \eta_1 \leq +1$  and  $-1 \leq \eta_2 \leq +1$  to an arbitrary piecewise smooth surface. Thus, the geometry is approximated by shape functions. It is not the subject of this paper to investigate the influence of these shape functions. It is assumed that all shape approximations in this paper are exact or include an error which may be neglected. In the practical application, this is ensured by using linear or quadratic polynomial shape functions. In general, an element with constant interpolation may be defined on a parabolic surface (superparametric approximation of the geometry). In other cases, a subparametric approximation is suitable, especially on plane surface areas.

Continuous elements account for the most commonly used types of boundary elements. Most likely, this is due to the experiences which users have made in the context of finite elements and, also, due to the misunderstanding that a continuous physical quantity, e.g. the sound pressure, should be approximated by continuous functions. Most popular elements are constructed by (bi)linear and (bi)quadratic Lagrangian interpolation functions.

Interpolation functions of continuous quadrilateral surface elements are easily constructed by multiplying two one-dimensional polynomials  $\psi_1$  and  $\psi_2$ , cf. [27]. Introducing the notation of upper indices  $l$  and  $q$  for linear and quadratic polynomials, respectively, these linear polynomials are formulated as

$$\begin{aligned} \psi_1^l(\eta_k) &= \frac{1}{2}(1 - \eta_k) & \text{and} \\ \psi_2^l(\eta_k) &= \frac{1}{2}(1 + \eta_k) \end{aligned} \quad (11.1)$$

whereas quadratic polynomials are given by

$$\begin{aligned} \psi_1^q(\eta_k) &= \frac{1}{2}\eta_k(1 - \eta_k) & , \\ \psi_2^q(\eta_k) &= \frac{1}{2}\eta_k(1 + \eta_k) & \text{and} \\ \psi_3^q(\eta_k) &= (1 - \eta_k^2) . \end{aligned} \quad (11.2)$$

Interpolation functions of discontinuous quadrilateral elements are constructed in a similar way. The simplest discontinuous elements use constant interpolation. Hence we write constant interpolation function as

$$\psi_1^c(\eta_k) = 1 . \quad (11.3)$$

For linear and quadratic discontinuous elements, we assume that the distance between the element edge and the closest nodal point on the standard element is given by the value of  $a$  with  $0 < a < 1$ . Introducing the constant  $\zeta = 1 - a$ , we write the

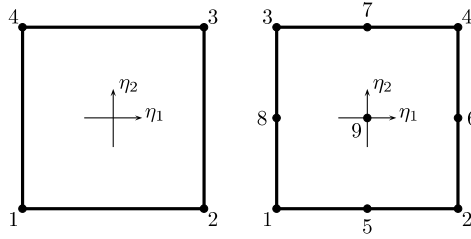


**Fig. 11.1** Linear (left) and quadratic (right) continuous quadrilateral elements.

$$\begin{aligned}\psi_1^l(\eta_k) &= \frac{1}{2\zeta} (\zeta - \eta_k) \quad \text{and} \\ \psi_2^l(\eta_k) &= \frac{1}{2\zeta} (\zeta + \eta_k)\end{aligned}\tag{11.4}$$

whereas quadratic polynomials are given by

$$\begin{aligned}\psi_1^q(\eta_k) &= \frac{1}{2\zeta^2} \eta_k (\eta_k - \zeta) \quad , \\ \psi_2^q(\eta_k) &= \frac{1}{2\zeta^2} \eta_k (\eta_k + \zeta) \quad \text{and} \\ \psi_3^q(\eta_k) &= \frac{1}{\zeta^2} (\zeta - \eta_k) (\zeta + \eta_k) \quad .\end{aligned}\tag{11.5}$$

The actual interpolation functions  $\varphi_l$  on the quadrilateral element are evaluated by multiplying the two one-dimensional polynomials  $\psi_i(\eta_1)$  and  $\psi_k(\eta_2)$ , cf. [27]. This gives the polynomials for constant quadrilaterals as

$$\varphi_1^c = \psi_1^c(\eta_1)\psi_1^c(\eta_2) = 1 \quad ,\tag{11.6}$$

for linear elements as

$$\begin{aligned}\varphi_1^l &= \psi_1^l(\eta_1) \psi_1^l(\eta_2) \quad , \quad \varphi_2^l = \psi_2^l(\eta_1) \psi_1^l(\eta_2) \quad , \\ \varphi_3^l &= \psi_2^l(\eta_1) \psi_2^l(\eta_2) \quad , \quad \varphi_4^l = \psi_1^l(\eta_1) \psi_2^l(\eta_2) \quad ,\end{aligned}\tag{11.7}$$

and analogously for quadratic quadrilateral elements as

$$\begin{aligned}\varphi_1^q &= \psi_1^q(\eta_1) \psi_1^q(\eta_2) \quad , \quad \varphi_2^q = \psi_2^q(\eta_1) \psi_1^q(\eta_2) \quad , \quad \varphi_3^q = \psi_2^q(\eta_1) \psi_2^q(\eta_2) \quad , \\ \varphi_4^q &= \psi_1^q(\eta_1) \psi_2^q(\eta_2) \quad , \quad \varphi_5^q = \psi_3^q(\eta_1) \psi_1^q(\eta_2) \quad , \quad \varphi_6^q = \psi_2^q(\eta_1) \psi_3^q(\eta_2) \quad , \\ \varphi_7^q &= \psi_3^q(\eta_1) \psi_2^q(\eta_2) \quad , \quad \varphi_8^q = \psi_1^q(\eta_1) \psi_3^q(\eta_2) \quad , \quad \varphi_9^q = \psi_3^q(\eta_1) \psi_3^q(\eta_2) \quad .\end{aligned}\tag{11.8}$$

Figures 11.1 and 11.2 show the locations of nodes on continuous and discontinuous quadrilateral elements, respectively. Throughout the computational examples we will indicate different polynomial degree and element types for quadrilaterals as follows:

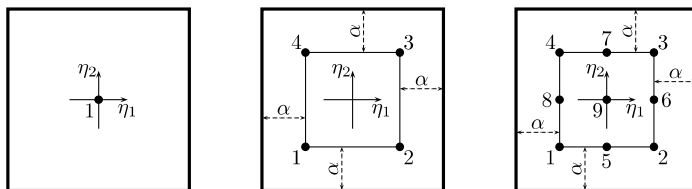


**Fig. 11.2** Constant (left), linear (middle) and quadratic (right) discontinuous quadrilateral elements.

- $P_0$  constant (discontinuous)
- $P_{1c}$  linear continuous
- $P_{1e}$  linear discontinuous, equidistant distribution of nodes ( $\alpha = 0.5$ )
- $P_{1L}$  linear discontinuous, nodes at zeros of Legendre polynomials ( $\alpha = 0.4226$ )
- $P_{2c}$  quadratic continuous
- $P_{2e}$  quadratic discontinuous, equidistant distribution of nodes ( $\alpha = 0.3333$ )
- $P_{2L}$  quadratic discontinuous, nodes at zeros of Legendre polynomials ( $\alpha = 0.2254$ )

Note that linear elements are actually bilinear elements since they involve a nonlinear term. Similarly, quadratic elements are actually biquadratic elements since higher order terms occur. The configurations of  $P_{1e}$  and  $P_{2e}$  produce an equidistantly distributed pattern of nodes on a regular mesh. In literature, this was recommended as a reasonable configuration for discontinuous elements, cf. [27, 28].

### 11.2.2 Triangular Elements

For triangular elements we use transformation from the standard interval  $0 \leq \gamma_1 \leq 1$  and  $0 \leq \gamma_2 \leq \gamma_1$  to an arbitrary smooth triangular surface element. Coordinate transformation and interpolation are done in an analogous way to quadrilateral elements. The details are different though. The parameter which is used to define the position of nodes on the element is called  $\beta$ .

In a similar way as for the quadrilateral elements, we start with introduction of one-dimensional polynomials. In contradiction to quadrilateral elements, at this stage, we will not distinguish between linear and quadratic elements. We introduce  $\gamma_3 = 1 - \gamma_1 - \gamma_2$  and

$$\psi_k(\gamma_k) = \frac{\gamma_k - \beta}{1 - 3\beta} \quad \text{for } k = 1, 2, 3. \tag{11.9}$$

The interpolation functions, however, require distinction into constant elements

$$\varphi_1^c = 1, \tag{11.10}$$

linear elements

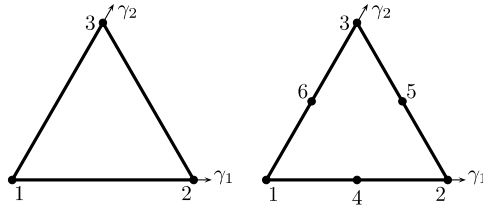


**Fig. 11.3** Linear (left) and quadratic (right) continuous triangular elements.

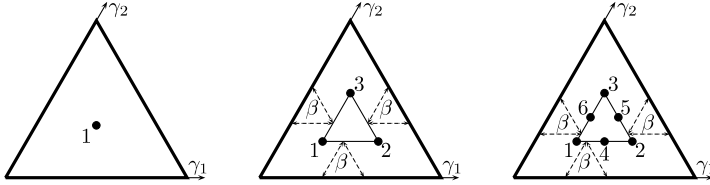


**Fig. 11.4** Constant (left), linear (middle) and quadratic (right) discontinuous triangular elements.

$$\begin{aligned}
 \varphi_1^l &= \psi_3(\gamma_3) , \\
 \varphi_2^l &= \psi_1(\gamma_1) , \\
 \varphi_3^l &= \psi_2(\gamma_2)
 \end{aligned}
 \tag{11.11}$$

and quadratic elements as

$$\begin{aligned}
 \varphi_1^q &= \psi_3(\gamma_3) [2\psi_3(\gamma_3) - 1] , & \varphi_4^q &= 4 \psi_1(\gamma_1) \psi_3(\gamma_3) , \\
 \varphi_2^q &= \psi_1(\gamma_1) [2\psi_1(\gamma_1) - 1] , & \varphi_5^q &= 4 \psi_1(\gamma_1) \psi_2(\gamma_2) , \\
 \varphi_3^q &= \psi_2(\gamma_2) [2\psi_2(\gamma_2) - 1] , & \varphi_6^q &= 4 \psi_2(\gamma_2) \psi_3(\gamma_3) .
 \end{aligned}
 \tag{11.12}$$

The node of a constant element is defined at the centroid of triangle, i.e.  $(\gamma_1, \gamma_2) = (1/3, 1/3)$ . The nodes of linear elements are located at  $(\beta, \beta)$  (1),  $(1 - 2\beta, \beta)$  (2) and  $(\beta, 1 - 2\beta)$  (3), whereas for quadratic elements, nodes 4–6 are assumed half way between the two nodes of 1–3 respectively, e.g. node 4 half way between 1 and 3. The nodal configurations of continuous and discontinuous triangular elements are shown in Figures 11.3 and 11.4 respectively. In a similar way as for the quadrilateral elements we use  $P_0$ ,  $P_{1c}$  and  $P_{2c}$ , whereas linear and quadratic discontinuous elements require further specifications as

- $P_{1e}$  linear discontinuous,  
equidistant distribution of nodes ( $\beta = 0.25$ )
- $P_{1L}$  linear discontinuous,  
nodes at zeros of Legendre polynomials ( $\beta = 0.1667$ )
- $P_{2e}$  quadratic discontinuous,  
equidistant distribution of nodes ( $\beta = 0.1667$ )
- $P_{2L}$  quadratic discontinuous,  
nodes at zeros of Legendre polynomials ( $\beta = 0.0916$ )

Note that orthogonal polynomials with respect to the weighting function 1 on a triangular domain are not called Legendre polynomials. We just keep this notation to compare with quadrilateral elements. Furthermore, note that the zeros of second order orthogonal polynomials with respect to the weighting function 1 on a triangular domain do not form a triangle. Actually, nodes 1–3 and 4–6 describe two triangles according to Figure 11.4. However, their location is well approximated by one triangle. To be exact [31], two values of  $\beta$  are required, i.e. for nodes 1–3 we have  $\beta = 0.0916$  whereas nodes 4–6 require  $\beta = 0.1081$ .

### 11.3 Error Measures

We define an error function  $e^\Gamma$  for the surface error as

$$e^\Gamma(\mathbf{x}) = \bar{p}(\mathbf{x}) - p(\mathbf{x}) \quad \mathbf{x} \in \Gamma \quad (11.13)$$

where  $\bar{p}(\mathbf{x})$  represents the approximate solution yielded by using the boundary element formulation and  $p(\mathbf{x})$  represents either the analytic solution of the one-dimensional duct problem or, in case of the sedan cabin, the solution which is obtained by the finest discretization using quadratic elements  $P_{2L}$ . An error  $e^\Omega$  is defined analogously in the interior domain, i.e. for  $\mathbf{x} \in \Omega$ .

The discrete error function is evaluated in discrete points, i.e. all collocation points for the surface error and 33 internal points for the error in the cavity, i.e. all points located in centroid of the cross section and equidistantly distributed along the length. Then, the discrete surface error is determined as

$$\|e^\Gamma\|_m = \left( \frac{1}{N_n} \sum_{i=1}^{N_n} \|e(\mathbf{x}_i)\|_m^m \right)^{\frac{1}{m}} \quad (11.14)$$

where  $N_n$  represents the number of nodes and  $m$  the specific norm, the Euclidean norm (rms) for  $m = 2$  and the maximum norm for  $m \rightarrow \infty$ .

Further, we use relative errors  $e_m^\Gamma$  for the sound pressure error

$$e_m^\Gamma = \frac{\|e^\Gamma\|_m}{\|p^\Gamma\|_m} \quad (11.15)$$

where  $\|p^\Gamma\|_m$  accounts for the discrete norm of the exact sound pressure. Analogously,  $e_m^\Omega$  accounts for the sound pressure error at 33 equally spaced points inside the duct.

An iterative solver is used for the linear system of equations. The residuum of  $10^{-8}$  which is demanded guarantees that the iterative solver does not essentially influence the error functions.

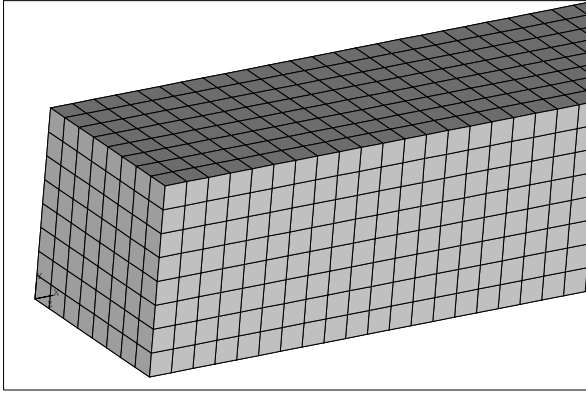


**Fig. 11.5** BE mesh of duct end,  $h_8$ .

## 11.4 Computational Example: Long Duct

### 11.4.1 Model Description and Error Measures

We consider an air-filled duct of length  $l = 3.4$  m and a  $0.2\text{m} \times 0.2\text{m}$  square cross section. Material data of air being  $\rho = 1.3 \text{ kg/m}^3$  and  $c = 340$  m/s, we expect one wave over the length at  $f = 100$  Hz. We assume  $Y = 0$  on the entire surface with the exception of  $Y(l) = (\rho c)^{-1}$ . Furthermore, for the particle velocity we use  $v_s = 0$  with the exception  $v_s(x = 0) = 1$  m/s where the coordinate  $x$  is used in the interval of  $0 \leq x \leq l$ . Since we want to compare solutions of the three-dimensional method with the analytical solution of the corresponding one-dimensional problem, it is necessary to apply zero boundary conditions for the boundary admittance and the particle velocity at all other surfaces.

The exact solution of the corresponding one-dimensional problem is given by

$$p(x) = -v_s(0) \rho c e^{ikx} . \quad (11.16)$$

The sound pressure magnitude is constant in the duct and over the entire frequency range. The solution may be considered as waves traveling through the duct. The boundary condition at  $x = l$  ensures that the wave is fully absorbed.

Although, a smooth solution is expected over the entire frequency range, the numeric solution is unstable if modes perpendicular to the traveling waves occur. For the above given cross section, these modes occur for frequencies of 850, 1700, 2550, 3400 Hz and higher. To present a smooth solution for higher frequencies, we compare with the additional example of a particular thin duct of  $0.025\text{m} \times 0.025\text{m}$  square cross section. There, perpendicular modes may be expected from 6800 Hz on. This corresponds to a wavenumber  $kl = 136\pi$ .

Several different meshes are considered. In what follows, we will use  $h_n$  to indicate element size. Subscript  $n$  counts the number of elements over the width of the duct. Figure 11.5 shows the  $h_8$ -mesh of the duct end. More detailed information

**Table 11.1** Comparison of mesh sizes (number of nodes and elements) for different element sizes, for continuous and discontinuous quadrilateral elements and for different polynomial degree of interpolation.

number of elements per length		ref. to	edge-length of element $h$ in [m]	polynomial degree $p$	number of elements	number of nodes for elements	
width						contin.	discontin.
17	1	$h_1$	0.2	0	70	72	70
				1			280
				2			630
34	2	$h_2$	0.1	0	280	282	280
				1			1120
				2			2520
51	3	$h_3$	0.0667	0	630	632	630
				1			2522
				2			5670
68	4	$h_4$	0.05	0	1120	1122	1120
				1			4480
				2			10080
102	6	$h_6$	0.0333	0	2520	2522	2520
				1			
136	8	$h_8$	0.025	0	4480	4482	4480
				1			
(thin)	1		0.025	0	546	548	546
136				1			2184
				2			4914

about mesh size, number of nodes and elements for different types of elements can be found in Table 11.1.

#### 11.4.2 Error in Terms of Location in the Duct

We start with investigating the error along the length of the duct. In Figure 11.6, we compare one line in models of  $P_0$ ,  $P_{1c}$  and  $P_{2c}$  elements. Using constant elements, we observe that the approximate solution of the sound pressure magnitude underestimates the exact solution over the whole length of the duct. The deviation varies rather little. In contrast to the solution with constant elements, linear elements provide a solution where the sound pressure magnitude is somewhat overestimated at one end and clearly underestimated at the other. Obviously, the ratio between maximum norm and Euclidean norm is greater for linear elements compared to constant elements.

Moreover, Figure 11.6 illustrates the difference between edges and smooth surfaces. Although, the problem is essentially one-dimensional, the sound pressure

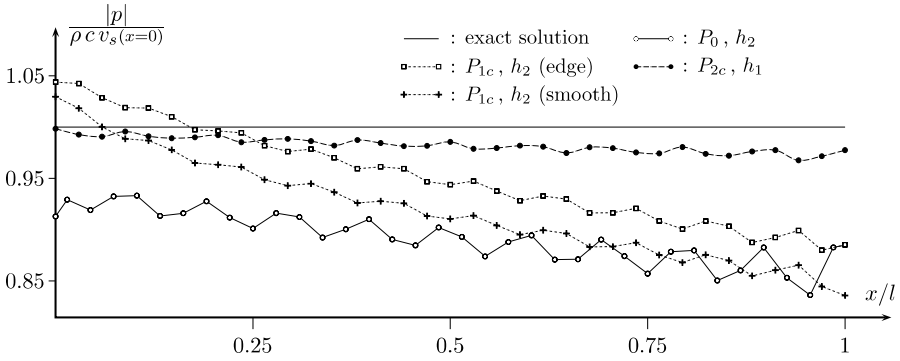


**Fig. 11.6** Sound pressure magnitude along lines on surface over the length of duct (collocation points marked) at  $f = 500$  Hz: Comparison of exact and numerical solutions using  $P_0$ ,  $P_{1c}$  and  $P_{2c}$  elements.

magnitude at collocation points on smooth surfaces is significantly smaller than at edge points. This observation holds for continuous elements only since discontinuous do not allow collocation points at edges. In Figure 11.6, this effect is only shown for linear elements since it is less significant for quadratic elements, cf. [18].

### 11.4.3 Error in Terms of Frequency

Figure 11.7 shows the error  $e_2^F$  for different meshes in terms of frequency. We observe similar errors and slopes for  $P_0$  and  $P_{1c}$  elements. It is common to write the error in the form

$$e^F(h, k) \sim C(h, \dots) k^\alpha. \tag{11.17}$$

For the  $P_{1L}$  elements, the error is much lower than for  $P_0$  and  $P_{1c}$  elements. However, we observe that for  $P_{1L}$  the error functions are quite flat up to a certain frequency. Above that frequency, these curves increase drastically. Most likely, the error dependence cannot be written in the form of Equation (11.17).

For  $P_{2c}$  elements, the error curves in terms of  $k$  are much steeper. Functions of error show lower rise for elements  $P_{2L}$ , especially if the error is of low level. In general, the error level is very low for elements  $P_{1L}$  and  $P_{2L}$ . This indicates that the theoretical prediction that collocation at the zeros of Legendre polynomials causes an effect of superconvergence, cf. Atkinson [2], seems to hold. Actually, it is just possible to identify a very low error but the superconvergence effect is not confirmed at this point.

In the lower right subfigure of Figure 11.7 the smoother functions of error of the thin duct are collected. All of these models consist of the same number of elements while the number of nodes differs significantly. It can be seen that more or less straight lines represent the error dependence upon  $k$  for the elements  $P_0, P_{1c}, P_{1e}, P_{2c}$  and  $P_{2e}$  provided that the error is less than 20 . . . 30%. When looking at the error dependence for  $P_{1L}$  and  $P_{2L}$  straight lines are observed for low errors.

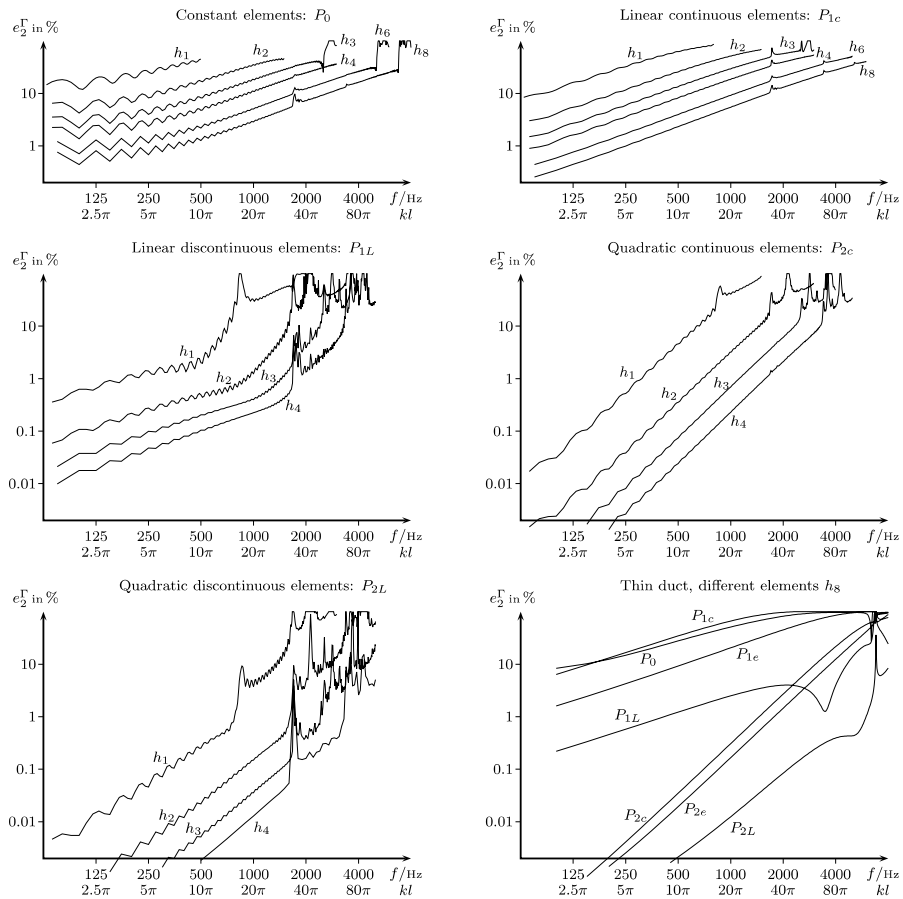


**Fig. 11.7** Long duct: Surface error in Euclidean norm in terms of frequency and wave number; resp., Lower right subfigure: Surface error for thin duct and different element types.

To our surprise, the error decreases significantly beyond 2000 Hz in the case of linear elements  $P_{1L}$ , whereas the error stagnates in a frequency range between 3500 and 6000 Hz for elements  $P_{2L}$ . These phenomena will be discussed later in this section when looking for an optimal location of nodal points on the element.

Efficiency of element types is compared for surface error in Euclidean norm and in maximum norm in Figure 11.8 and Figure 11.9, respectively. Based on the assumption that the number of nodes mainly controls the computational costs (memory and CPU time), we compare different meshes of the same degree of freedom being 2520 or 2522, cf. Table 11.1. When considering the error in the Euclidean norm, quadratic elements  $P_{2L}$  prove to be most efficient. Quadratic elements  $P_{2c}$  and  $P_{2e}$  perform well too. However, linear elements  $P_{1L}$  prove to perform efficiently if very low errors are desired. Furthermore, it can be seen that constant elements are as efficient as discontinuous linear elements  $P_{1e}$  and provide lower errors than continuous linear

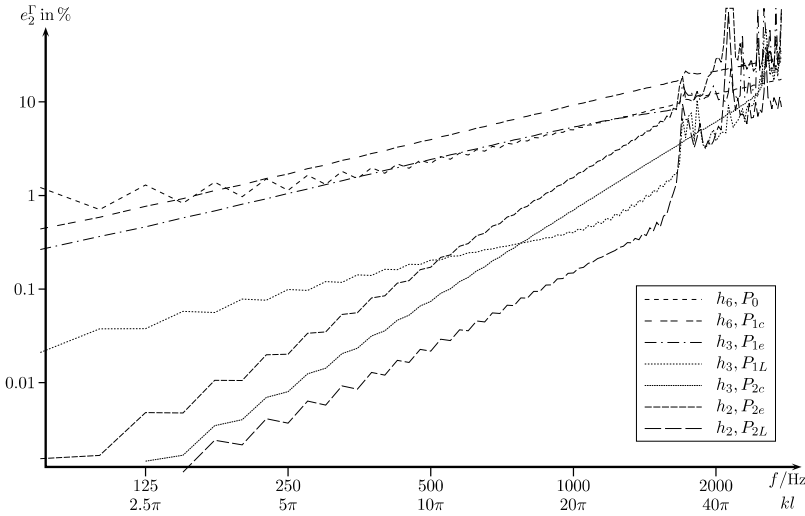


**Fig. 11.8** Long duct, surface error in Euclidean norm: Comparison of different element types. Note, that all models have the same degree of freedom of approx. 2520.

elements  $P_{1c}$ . We observe a slightly different behaviour when the error is measured in the maximum norm, cf. Figure 11.9. Then, quadratic elements  $P_{2L}$  and  $P_{2c}$  give about the same error, whereas elements  $P_{2e}$  come out with larger errors. Again, linear elements  $P_{1L}$  give very low errors compared with linear elements  $P_{1e}$  and  $P_{1c}$ . The latter have larger errors than constant elements  $P_0$ .

Based on the results of this chapter there is no indication of a pollution effect for boundary element collocation method. We will review this problem in the subsequent subsection again.

In the papers [18, 22], the reader finds additional graphs on error in terms of frequency. These include comparisons of quadrilaterals and triangles, where hardly any difference could be observed. Further, the differences of errors in Euclidean and in maximum norms are compared. More detailed comparisons of surface error and field point errors are shown.

#### 11.4.4 Error in Terms of Element Size

The computational example in Ref. [18] confirmed the effect of superconvergence for regular meshes and even polynomial degree of the interpolation functions. Following Atkinson’s prediction [2] we should expect an error dependence as

$$e^{\Gamma}(h, k) \sim C(k, \dots) h^{p+1} \tag{11.18}$$

where  $p$  is the polynomial degree. For a regular mesh of constant or continuous elements of even number of polynomial degree of the interpolation functions, we can expect an additional factor of  $h$  in the error dependence as

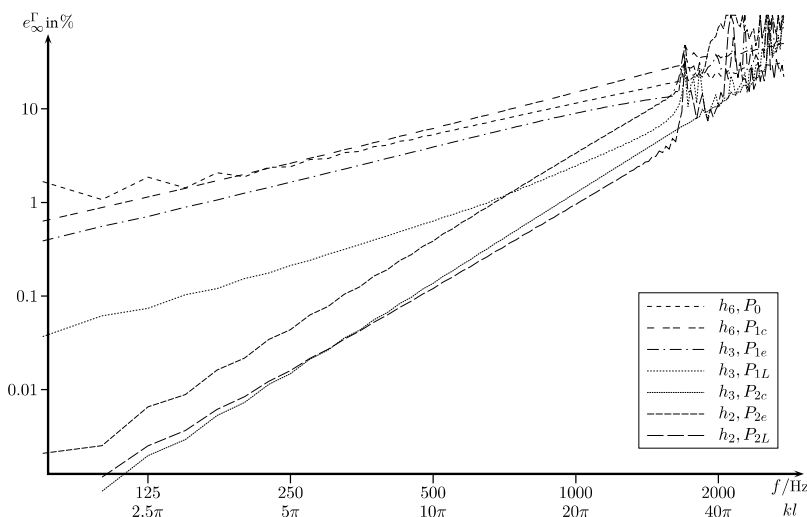


**Fig. 11.9** Long duct, surface error in maximum norm: Comparison of different element types. Note, that all models have the same degree of freedom of approx. 2520.

$$e^r(k, h) \sim C_h(k, \dots) h^{p+2}, \quad p = 0, 2, 4, \dots \quad (11.19)$$

The higher exponents  $\beta$  for regular meshes of constant or continuous elements of even polynomial degree are valid for the Euclidean norm measured in the discrete collocation points only. If we consider the error measured in the Euclidean norm over the entire surface we would observe an error behaviour as given in (11.18).

The effect of superconvergence at collocation points is well documented in the literature, see for example Hackbusch [10]. There, the superconvergence effect is reported for arbitrary meshes of constant elements. This coincides with the observation [2, 5, 6] indicating that the effect of superconvergence may be achieved on arbitrary meshes of discontinuous Lagrange elements with nodal point at the zeros of orthogonal polynomials, e.g. Legendre polynomials.

Error dependence in terms of the element size is presented for two different frequencies in Figure 11.10. We easily realize that different functions of error occur for different frequencies. For 500 Hz, lines for  $P_0, P_{1e}, P_{1c}$  and  $P_{1L}$  are almost parallel but on different levels. The remaining three functions are almost parallel too but much steeper. For 1500 Hz, the lines for  $P_0, P_{1e}$  are  $P_{1c}$  parallel. The error for elements  $P_{1L}$ , however, is now parallel to the lines of quadratic elements which indicates higher convergence rate for these higher frequencies. Note, that functions of error for  $P_{1L}$  and  $P_{2e}$  coincide!

So we realize that slopes of error for  $P_{1L}$  are about the same as for other linear or for constant elements at the low frequency of 500 Hz but much greater for the higher frequency of 1500 Hz. A similar behaviour is assumed for quadratic elements  $P_{2L}$ . The frequency is not large enough to confirm. (Solutions at higher frequencies are perturbed due to the ill-conditioning of perpendicular modes.)

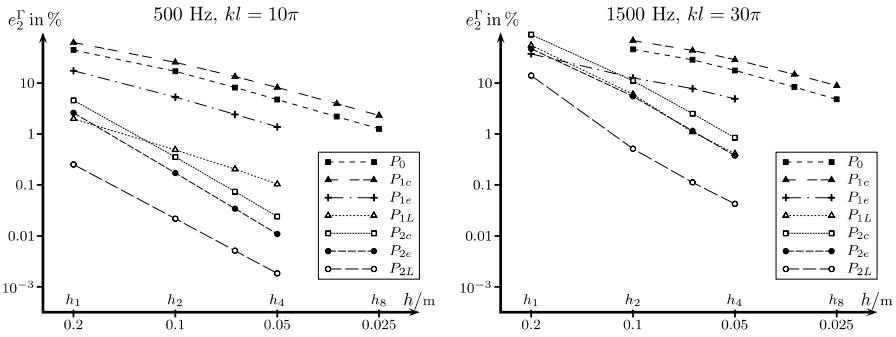


Fig. 11.10 Long duct, surface error in Euclidean norm, error in terms of element size.

Since the error functions in terms of mesh size show the same slopes at least for the  $P_0, P_{1e}, P_{1c}, P_{2c}$  and  $P_{2e}$  elements, we assume that an occurrence of a pollution effect which is well-known from finite elements [13] is very unlikely. In the subsequent subsection, we will discuss why the slopes of error functions of  $P_{1L}$  and  $P_{2L}$  elements show or may show a dependence on frequency.

### 11.4.5 Error in Terms of Location of Collocation Points

In this subsection, the location of nodal points is investigated. It became obvious in the previous subsections that location of nodes at the zeros of Legendre polynomials provides lower errors compared to an equidistant distribution of nodes on the surface. According to Atkinson, it is not required to put nodes at the zeroes of Legendre polynomials. More general, nodes should be located at zeroes of orthogonal functions being defined on the standard interval  $[-1, 1]$ . Legendre polynomials account for the simplest selection of orthogonal functions since they are well-known and particularly designed for the interval  $[-1, 1]$ . In what follows, it will be investigated if the zeros of the Legendre polynomials actually account an optimal position of nodes.

Figure 11.11 contains the errors  $e_2^{\Gamma}$  and  $e_2^{\Omega}$  in terms of  $\alpha$ . Our test model  $h_2$  consists of 280 elements. We expect the lowest error at  $\alpha = 0.4226$  for linear elements and at  $\alpha = 0.2254$  for quadratic elements. Although not exactly fulfilled we see that an optimal location of nodal values is very close to the zeros of the Legendre polynomials. The optimal value varies with frequency. For low frequencies and low error, lower values of  $\alpha$  account for an optimal position, for higher frequencies and, consequently, higher errors an  $\alpha$  greater than that providing the zeros of the Legendre polynomials is required for optimal elements. In between, a large frequency range is observed where nodal points are optimally placed as predicted [2, 5, 6].

Actually, the optimal location of nodes at the zeros of Legendre polynomials refers to pure Neumann problems using the double layer potential operator. Herein, a mixed problem is considered because a Robin boundary condition is applied at one end of the duct. Apparently, the choice of nodes at the zeros of the Legendre polynomials is a good approximation of the optimal location. In case of other operators,

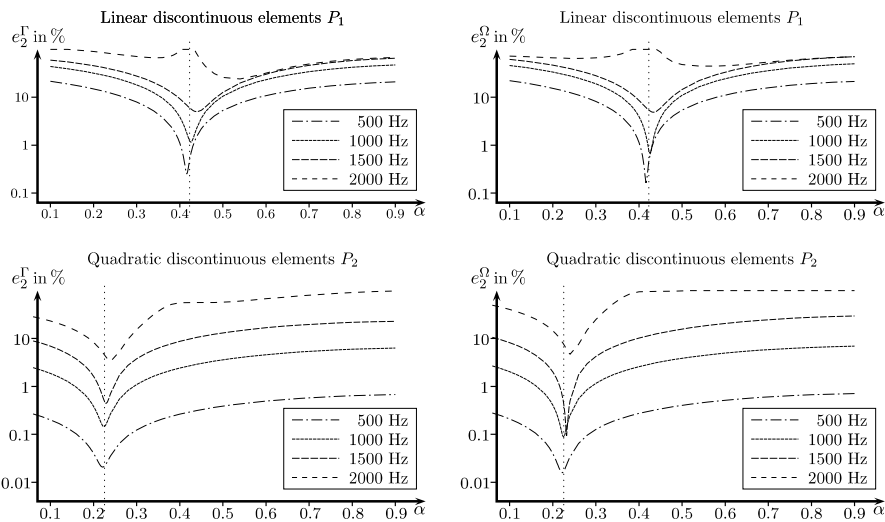


**Fig. 11.11** Long duct, quadrilateral elements, surface error and error at internal points in Euclidean norm, error in terms of the position of nodal points on elements.

i.e. the hypersingular operator, and other boundary conditions, the optimal position of nodes may differ from the one identified here.

It shall be mentioned at this point that for certain frequencies extremely low errors are gained for field points compared to surface error. The most remarkable example is found for quadratic elements at 1500 Hz. However, significant differences can be found at 500 and 1000 Hz for both, linear and quadratic elements. The error of the solution at the surface and at internal points is almost the same for very low and for higher frequencies.

The fact that the optimal location of nodal points varies with frequency explains the error behaviour for the thin duct, cf. lower right subfigure of Figure 11.7. There, we have observed decreasing error for increasing frequency in certain ranges. It does further explain why error dependence upon element size changes with frequency.

In Table 11.2, the error  $e_2^\Gamma$  is compared for continuous and discontinuous elements. The third column contains the numeric error of the  $h_2$  discretization of continuous elements which is the same element size as for the discontinuous elements. The fourth column contains the error of the  $h_4$  discretization of continuous elements which results in (approximately) the same degree of freedom as for the discontinuous elements. These results confirm that the node location at the Legendre zeros and, even better, the optimal location give much more accuracy for linear elements and, mostly, better accuracy for quadratic elements.

By now, our considerations were limited to quadrilateral elements. When looking at the error in terms of node position it is necessary to investigate triangles separately. For that, we create a mesh of triangles simply by dividing each quadrilateral into two triangles. Starting with the element size  $h = 0.1m$  we yield 560 triangles. Linear and quadratic discontinuous elements give 1680 and 3360 nodes, respectively.

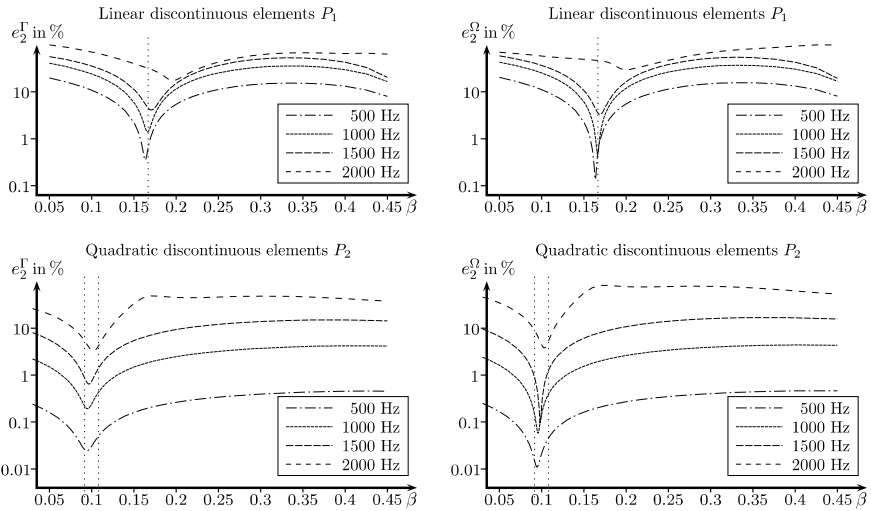


**Fig. 11.12** Long duct, triangular elements, surface error and error at internal points in Euclidean norm, error in terms of the position of nodal points on elements.

**Table 11.2** Long duct, quadrilateral elements,  $e_2^f$  in %, comparison between continuous (different element size) and discontinuous elements (different location of nodes).

$p$	$f$ [Hz]	continuous elements		discontinuous elements $h_2$ , location of nodes		
		$h_2$	$h_4$	equidistant	Legendre zeros	best solution
1	100	4.1	1.2	0.82	0.11	0.032
	500	25.6	8.2	5.3	0.49	0.25
	1000	51.3	18.5	10.5	1.24	1.16
	1500	68.7	28.8	12.7	6.04	5.0
	2000	—	39.3	26.0	100	24.2
2	100	0.0024	0.0002	0.0017	0.0004	0.0003
	500	0.35	0.024	0.17	0.021	0.021
	1000	3.2	0.23	1.55	0.15	0.145
	1500	11.1	0.85	5.49	0.51	0.446
	2000	37.3	2.1	28.7	4.66	3.37

Figure 11.12 supplies estimates for optimal location of nodal points in triangles. The results confirm the prediction that the optimal position is at  $\beta = 0.1667$  on linear elements and in the interval  $0.0916 \leq \beta \leq 0.1081$ . A value of  $\beta \approx 0.098$  is identified as the optimum. Similar to quadrilateral elements, we observe a particular gain in accuracy for internal points at certain frequencies. These frequencies coincide with those reported for quadrilateral elements.

As a conclusion for this subsection we want to emphasize that the position of nodal points on the element can influence the accuracy of the solution by one to two orders of magnitude.

**Table 11.3** Comparison of mesh sizes (number of nodes and elements) for different element sizes, triangular and quadrilateral elements and for different polynomial degree of interpolation.

maximum elem. size $h$ in [m]	polynom. degree $p$	number of elem.	number of triang.	number of quadril.	number of nodes elements contin. discontin.	
0.4	0					258
	1	258	104	154	208	928
	2				826	2010
0.2	0					604
	1	604	128	476	542	2288
	2				2162	5052
0.1	0					1774
	1	1774	74	1700	1739	7022
	2				6950	15744
0.05	0	5738	24	5714		5738
	1				5728	

## 11.5 Computational Example: Sedan Cabin Compartment

This example is chosen to examine an irregular mesh which is the result of an automatic mesh generation. Four meshes are investigated. The meshes contain quadrilaterals and triangles. Their detailed data are given in Table 11.3. A more vivid description of these models is shown in Figure 11.13. For discontinuous elements with nodes at zeroes of the Legendre polynomials,  $P_{1L}$  and  $P_{2L}$ , we distinguish between triangles and quadrilaterals as discussed in the previous section.

A fictitious excitation with uniform normal particle velocity  $\bar{v}_s = 1$  mm/s at the lower left front area is applied, cf. Figure 11.13. A uniform boundary admittance of

$$Y = \frac{1}{\rho c} \frac{f}{f_0} \quad (f_0 = 2800 \text{ Hz}) \quad (11.20)$$

is applied to simulate the absorbing behaviour of the surfaces inside the cabin [21]. This value corresponds to experimental measurements of the reverberation time and a corresponding average absorption coefficient. The sound pressure is computed at ten points inside the cabin.

It shall be mentioned that the author is aware that realistic calculations of cabin noise problems are done for frequencies up to (max.) 150. . .200 Hz. However, the major uncertainty of these calculations are structural transfer functions and realistic distributions of the boundary admittance values. We will show that even a coarse boundary element mesh for the fluid can give an excellent approximation of the sound pressure field over the entire frequency range.

Our reference solution is computed by using discontinuous quadratic elements of size  $h \leq 0.1$  m. As indicated by Table 11.3, the associated system of equations has

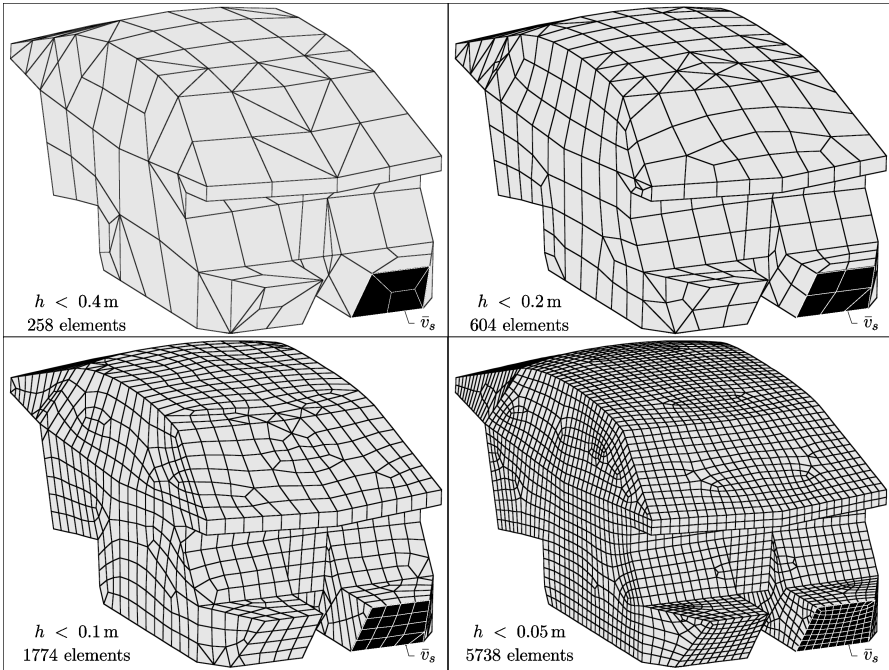


**Fig. 11.13** Four meshes of sedan cabin compartment, element size with upper limits, indication of excitation area by particle velocity  $\bar{v}_s$ .

15744 unknowns. In what follows, we will call this solution our reference solution and all errors are evaluated with respect to this reference.

The left subfigure of Figure 11.14 shows the sound pressure level at an arbitrarily chosen internal point for different meshes. All transfer functions are in good agreement for frequencies lower than 100 Hz. Above that, the solution of  $p = 0$  deviates from the others but maxima and minima of the transfer functions are found at correct frequencies up to about 350 Hz. Unlike the case of uniform mesh, linear elements provide a better approximation of the sound pressure level in the present application. However, even by using such a coarse mesh, the general approximation is good. Quadratic elements hardly allow us to find differences between the different solutions. In the right subfigure of Figure 11.14, we observe hardly any differences between the different sound pressure level curves.

Looking at the error at internal points in terms of element size, Figures 11.15 and 11.16 show the error functions for different types of elements and different frequencies. Most of these functions are virtually linear but not necessarily parallel for the same element type, cf. Figure 11.15. The comparison of different element types confirms excellent performance of discontinuous elements, cf. Figure 11.16. So, we realize that, in this example, constant elements give lower error than continuous linear elements. Furthermore, discontinuous linear elements give lower error

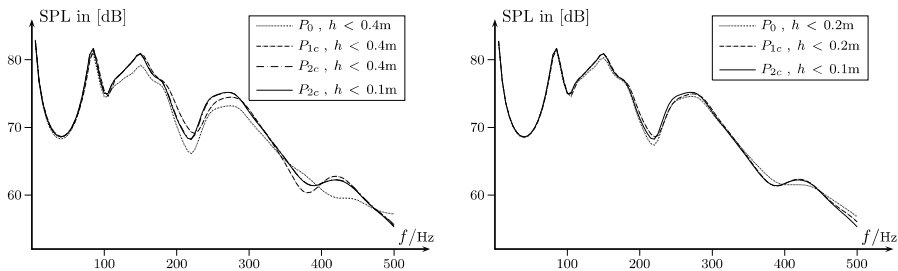


**Fig. 11.14** Sound pressure level inside the cabin, location: passenger ear in the rear, different meshes, different polynomial degree of interpolation.

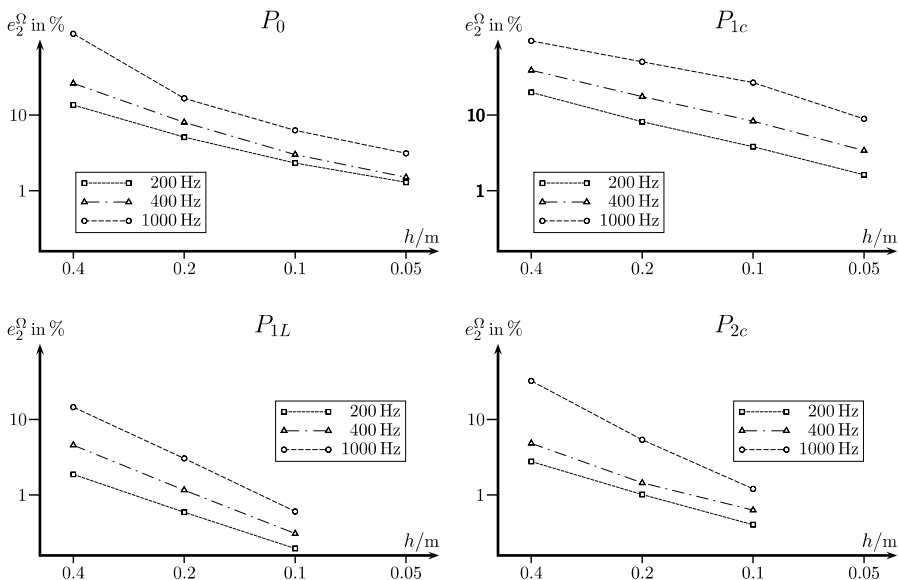


**Fig. 11.15** Sedan cabin, error at ten internal points in terms of element size for different frequencies, subfigures show behaviour for different types of elements.

than continuous quadratic elements. Note, that this presumes that a solution using discontinuous quadratic elements provides the lowest error.

In the next step, we investigate the error in terms of location of nodal points. For that, we use the parameter  $\alpha$  for quadrilaterals, Figure 11.2, and  $\beta$  for triangles, Figure 11.4. To use only one variable, it is assumed that  $\alpha = 2\beta$ . The model for  $h \leq 0.2m$  consists of 476 quadrilaterals and 128 triangles. As we have seen for the duct's regular meshes either consisting of quadrilaterals or of triangles, optimal values of  $\alpha$  and  $2\beta$  are different. Figure 11.17 shows that significant improvements can be reported in the vicinity of  $0.35 \leq \alpha \leq 0.42$  for linear and  $\alpha \approx 0.2$  for quadratic elements.

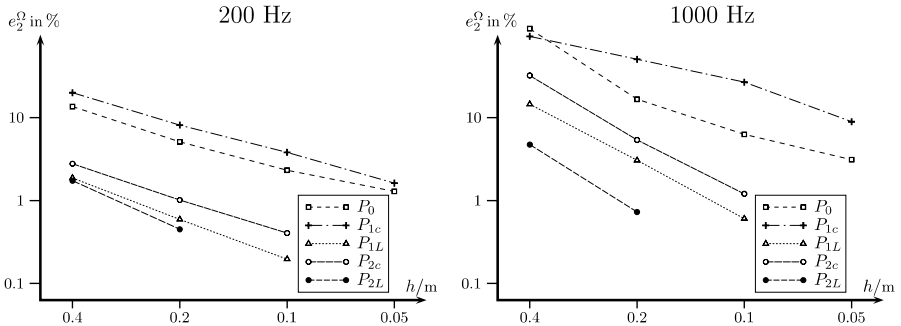


**Fig. 11.16** Sedan cabin, error at ten internal points in terms of element size for different element types, subfigures show behaviour for different frequencies.

For linear elements, a discontinuity is observed at lower frequencies at about  $\alpha = 0.35$ . The author could not find a reasonable explanation for this phenomenon. Originally thought to be caused by the integration scheme, integration was performed extremely accurate, i.e. number of integration points for Gauss–Legendre quadrature controlled by distance between element and source point varied between  $8 \times 8$  and  $30 \times 30$  on single element. Polynom transformation [34] is applied for nearly singular integrals.

Another unexpected result is found for quadratic elements at 250 Hz. There, the error appears virtually insensitive with respect to the location of nodes.

### 11.6 Conclusions

This paper has reviewed the results of two former papers [18, 22]. Continuous and discontinuous Lagrangian boundary elements are compared for the collocation method.

It could be shown for these low order elements that discontinuous elements perform more efficient than continuous ones if nodal points are located at the zeros of the Legendre polynomials. To achieve very low errors, the use of discontinuous quadratic elements is recommended. If a larger error is accepted, discontinuous linear or even constant elements can be efficiently used. The most commonly used linear continuous elements seem to be the most unreliable and inefficient element type of those which have been tested here.

The author has presented tables for the long duct example. These tables show how many elements  $P_0$ ,  $P_{1c}$  and  $P_{2c}$  are required to remain below a certain error. They confirm that six linear boundary elements correspond to 10...15 percent error whereas the same number of constant elements correspond to approximately 10 percent error. The same result is achieved when using approximately two  $P_{2c}$  elements per wavelength. However, the author recommends to use finer meshes in particular if the mesh is not regular and if it contains edges and corners with geometric or other singularities.

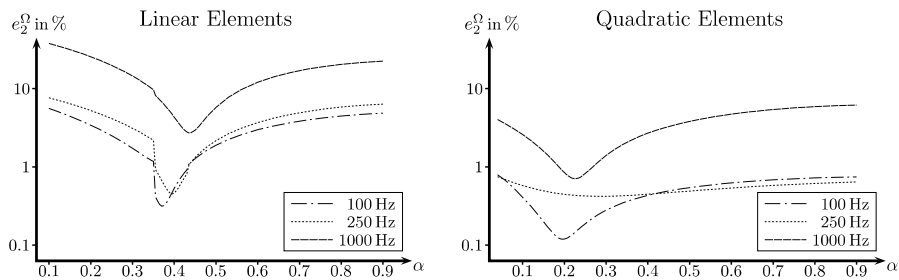


**Fig. 11.17** Sedan cabin, error at ten internal points in terms of location of nodes.

In the example of the long duct and, in particular, in the example of the thin duct, we could not find any indication of a pollution effect in the frequency range of  $0 \leq kl \leq 160\pi$ . Consequently, a discretization rule of using a fixed number of elements per wavelength remains acceptable for the boundary element collocation method. When looking at the error in terms of location of the nodes on the elements, we found that this can influence the error by one or two orders of magnitude. This could even be shown for the irregular mesh of the sedan cabin compartment.

In addition to the remarkable gain in efficiency for discontinuous elements, it shall be mentioned that they possess a number of interesting features as

- they are well suited for adaptive mesh refinement,
- they fulfill  $C^1$  continuity condition at collocation points which is required for the hypersingular formulation,
- they simplify construction of mesh dependent preconditioners for iterative solvers, and
- they are well suited for development of parallel codes.

Finally concluding, we strongly recommend the use of discontinuous boundary elements with nodes located at the zeros of the Legendre polynomials provided our problem is essentially related to inversion of the double layer potential operator. In case of mixed problems and when using the hypersingular operator, it is likely that other optimal locations of nodes will be found.

## References

1. Araujo FC, Silva KI, Telles JCF (2006) Generic domain decomposition and iterative solvers for 3D BEM problems. *International Journal for Numerical Methods in Engineering* 68:448–472
2. Atkinson KE (1997) *The Numerical Solution of Integral Equations of the Second Kind*. Cambridge University Press, Cambridge
3. Branski A (1997) Model of an acoustic source with discontinuous optimal elements. *Archives of Acoustics* 22:383–395
4. Burton AJ, Miller GF (1971) The application of integral equation methods to the numerical solution of some exterior boundary-value problems. *Proceedings of the Royal Society of London* 323:201–220

5. Chandler G (1979) Superconvergence of numerical solutions to second kind integral equations. PhD Thesis, Australian National University, Canberra
6. Chatelin F, Lebbar R (1981) The iterated projection solution for the fredholm integral equation of the second kind. *Journal of the Australian Mathematical Society, Series B* 22:439–451
7. Ciskowski RD, Brebbia CA (eds) (1991) *Boundary Elements in Acoustics*. Computational Mechanics Publications and Elsevier Applied Science, Southampton–Boston
8. Estorff O von (ed) (2000) *Boundary elements in acoustics: Advances and applications*. WIT Press, Southampton
9. Florez WF, Power H (2001) Comparison between continuous and discontinuous boundary elements in the multidomain dual reciprocity method for the solution of the two-dimensional Navier–Stokes equation. *Engineering Analysis with Boundary Elements* 25:57–69
10. Hackbusch W (1995) *Integral Equations: Theory and Numerical Treatment*, Birkhäuser–Verlag, Basel–Boston–Berlin
11. Harari I, Grosh K, Hughes TJR, Malhotra M, Pinsky PM, Stewart JR, Thompson LL (1996) Recent development in finite element methods for structural acoustics. *Archives of Computational Methods in Engineering* 3:131–309
12. Harari I, Hughes TJR (1992) A cost comparison of boundary element and finite element methods for problems of time–harmonic acoustics. *Computer Methods in Applied Mechanics and Engineering* 97:77–102
13. Ihlenburg F (1998) *Finite element analysis of acoustic scattering*. Springer–Verlag, New York
14. Jerry AJ (1977) The Shannon sampling theorem – it various extensions and applications: A tutorial review. *Proceedings of the IEEE* 65:1565–1596
15. Kirkup SM (1998) The boundary element method in acoustics. *Integrated Sound Software*, Heptonstall
16. Makarov SN, Ochmann M (1998) An iterative solver for the Helmholtz integral equation for high frequency scattering. *Journal of the Acoustical Society of America* 103:742–750
17. Manolis GD, Banerjee PK (1986) Conforming versus non–conforming boundary elements in three–dimensional elastostatics. *International Journal for Numerical Methods in Engineering* 23:1885–1904
18. Marburg S (2002) Six elements per wavelength. Is that enough? *Journal of Computational Acoustics* 10:25–51
19. Marburg S (2005) Normal modes in external acoustics. Part I: Investigation of the one-dimensional duct problem. *Acta Acustica united with Acustica* 91:1063–1078
20. Marburg S, Amini S (2005) Cat’s eye radiation with boundary elements: Comparative study on treatment of irregular frequencies. *Journal of Computational Acoustics* 13: 21–45
21. Marburg S, H.–J. Hardtke (1999) A study on the acoustic boundary admittance. Determination, results and consequences. *Engineering Analysis with Boundary Elements* 23:737–744
22. Marburg S, Schneider S (2003) Influence of element types on numeric error for acoustic boundary elements. *Journal of Computational Acoustics* 11:363–386
23. Marburg S, Schneider S (2003) Performance of iterative solvers for acoustic problems. Part I: Solvers and effect of diagonal preconditioning. *Engineering Analysis with Boundary Elements* 27:727–750
24. Meyer WL, Bell WA, Zinn BT, Stallybrass MP (1978) Boundary Integral Solutions of Three Dimensional Acoustic Radiation Problems. *Journal of Sound and Vibration* 59:245–262

25. Natalini B, Popov V (2007) On the optimal implementation of the boundary element dual reciprocity method—multi domain approach for 3d problems. *Engineering Analysis with Boundary Elements* 31:275–287
26. Patterson C, Sheikh (1984) Interelement continuity in the boundary element method. In: Brebbia CA (ed) *Topics in Boundary Element Research Vol 1: Basic Principles and Applications*. Chapter 6. Springer–Verlag, Berlin–Heidelberg–New York
27. Rego Silva Jd (1993) *Acoustic and elastic wave scattering using boundary elements*. Computational Mechanics Publications, Southampton–Boston
28. Rego Silva Jd, Wrobel LC, Telles JCF (1993) A new family of continuous/discontinuous three–dimensional boundary elements with application to acoustic wave propagation. *International Journal for Numerical Methods in Engineering* 36:1661–1679
29. Schmiechen P (1997) *Travelling wave speed coincidence*. PhD Thesis, Imperial College of Science, Technology and Medicine, University of London
30. Schneider S (2003) Application of fast methods for acoustic scattering and radiation problems. *Journal of Computational Acoustics* 11:387–401
31. Stroud AH (1971) *Approximate calculation of multiple integrals*. Prentice–Hall, Englewood Cliffs
32. Tadeu A, Antonio J (2000) Use of constant, linear and quadratic boundary elements in 3d wave diffraction analysis. *Engineering Analysis with Boundary Elements* 24:131–144
33. Tadeu AJB, Godinho L, Santos P (2001) Performance of the BEM solution in 3D acoustic wave scattering. *Advances in Engineering Software* 32:629–639
34. Telles JCF (1987) A self–adaptive coordinate transformation for efficient numerical evaluation of general boundary element integrals. *International Journal for Numerical Methods in Engineering* 24:959–973
35. Tsinopoulos SV, Agnantiaris JP, Polyzos D (1999) An advanced boundary element/fast Fourier transform axisymmetric formulation for acoustic radiation and wave scattering problems. *Journal of the Acoustical Society of America* 105:1517–1526
36. Wu TW (ed) (2000) *Boundary element acoustics: Fundamentals and computer codes*. WIT Press, Southampton
37. Wu TW, Cheng CYR (2003) Boundary element analysis of reactive mufflers and packed silencers with catalyst converters. *Electronic Journal of Boundary Elements* 1:218–235
38. Wu TW, Seybert AF, Wan GC (1991) On the numerical implementation of a cauchy principal value integral to insure a unique solution for acoustic radiation and scattering. *Journal of the Acoustical Society of America* 90:554–560
39. Wu TW, Wan GC (1992) Numerical modeling of acoustic radiation and scattering from thin bodies using a Cauchy principal integral equation. *Journal of the Acoustical Society of America* 92:2900–2906
40. Zhang XS, Ye TQ, Ge SL (2001) Several problems associated with discontinuous boundary elements. *Chinese Journal of Computational Mechanics* 18:331–334



<http://www.springer.com/978-3-540-77447-1>

Computational Acoustics of Noise Propagation in Fluids

- Finite and Boundary Element Methods

Marburg, S.; Nolte, B. (Eds.)

2008, XIII, 578 p., Hardcover

ISBN: 978-3-540-77447-1